

SPECTRAL PHASE: FROM BASICS TO VIDEO-RATE APPLICATION TO TUNING-FORK RESONANCE CHARACTERIZATION

* Patrick Sandoz ** Freddy Torrealba Anzola

Recibido: 05/12/2014 Aprobado: 07/03/2015

Abstract

Whereas graduated students are usually familiar with Fourier spectra, the spectral phase remains often mysterious to them. This paper proposes a “hands on” approach of discrete Fourier transform (DFT) and spectral phase. In a first part, basics of DFT are explored through elementary simulations. The variation of digital parameters allows the identification of sampled frequencies as well as their relation with the size of the sampled window. The significance of the spectrum phase is also illustrated experimentally to demonstrate the useful relationship between a displacement and the spectral phase. In a second part, these properties are put in application for the characterization of tuning-fork resonance by means of video-rate analysis of the spectral phase. Experimental hardware is reduced to elementary devices and remains affordable while involving all aspects of a measurement chain. The proposed progression constitutes a practical approach to discrete Fourier transform and spectral phase properties. At the end, the resonance curve of a tuning-fork is recorded in only a few minutes. The Shannon sampling theorem as well as the uncertainty relation linking the resolutions achieved in the direct and reciprocal domains, are also considered practically throughout this work.

Keywords: Fast Fourier Transform, Fourier Phase, tuning fork.

* *Département de Mécanique Appliquée R. Chaléat, Institut FEMTO-ST, UMR CNRS 6174, Université de Franche-Comté, 24, rue de l'Épitaphe, 25000 Besançon, FRANCE, patrick.sandoz@univ-fcomte.fr*

** *Universidad Centrocidental “Lisandro Alvarado”, Decanato de Ciencias y Tecnología, Depto. de Física, UICM, Av. Las Industrias Km. 1, Barquisimeto 3001, Venezuela, ftorre@ucla.edu.ve.*

FASE ESPECTRAL: DE LAS IDEAS BÁSICAS A LA APLICACIÓN EN UN VIDEO DE LA RESONANCIA DE UN DIAPASÓN

Resumen

Mientras que los estudiantes graduados están familiarizados con el espectro de Fourier, la fase espectral a menudo se mantiene misteriosa. Este artículo propone una aproximación práctica a la Transformada de Fourier Discreta (TFD) y a la fase espectral. En una primera parte, se exploran las bases de TFD mediante simulaciones elementales. La variación de parámetros digitales permite la identificación de frecuencias de muestreo y su relación con el tamaño de la ventana muestreada. La importancia del espectro de fase también se ilustra experimentalmente para demostrar la utilidad de la relación existente entre un desplazamiento y la fase espectral. En la segunda parte, estas propiedades son puestas en práctica caracterizando la resonancia de un diapasón mediante el análisis de la tasa de video de la fase espectral. El material experimental implicado en todos los aspectos de las medidas se reduce a unos dispositivos elementales y económicos. La propuesta constituye un acercamiento práctico a Transformada de Fourier Discreta y las propiedades de la fase espectral. Para finalizar, se registra la curva de resonancia de un diapasón en sólo unos minutos. El teorema del muestreo de Shannon, así como la relación de incertidumbre que liga las resoluciones alcanzadas en los dominios directos y recíprocos también son considerados prácticamente en todas las partes de este trabajo.

Palabras clave: Transformada de Fourier, Fase de Fourier, diapasón.

1. Introduction

Fourier transform is a key-concept to be transmitted in the frame of linear system theory (Oppenheim y Schafer, 1975). While time is usefully spend for teaching Fourier transform theory and its applications, some points remain often obscure in practice. Indeed several steps have to be clearly understood to pass from the general definition of the Fourier transform of continuous variables to the computer processing of experimental signals sampled over finite time intervals. Whereas the shape of the power spectrum obtained is usually well interpreted, the conversion of digital indexes into actual magnitudes of physical parameters is often difficult and the meaning of the Fourier phase remains widely misunderstood. Several papers published during the last decades have proposed useful application works for

the experimental approach of the Fourier transform (Higgins, 1976; Maas, 1978; D'Astous y Blanchard, 1982; Matthys y Pedrotti, 1982; Lambert y O'Driscoll, 1985; Kocher, 1988; Chen, Huang, y Loh, 1988; Whaite y Wolfe, 1990; Peters, 1992). Our aim is also to provide the frame of a laboratory work suited to make the students more familiar with these practical aspects of the Fourier transform; especially with the Fourier phase. This paper is made of two complementary parts. The first one is based on elementary digital simulations built in such a way that the meaning of the different parameters to be clarified is approached qualitatively through results displayed on the screen. This part allows the understanding of basic parameters and relationships:

- The frequencies actually sampled by a discrete Fourier transform as a function of the number of signal samples available. We emphasize on their property to correspond to a whole number of periods over the signal interval considered.
- The significance of these sampled frequencies with respect to the actual signal spectrum is discussed; especially in regards of the Shannon sampling theorem and of the effect of sampling on the signal Fourier spectrum.
- The meaning of the Fourier phase; i.e. the argument of each spectral component with respect to the corresponding analysis function. The ability of the Fourier phase to encode a delay is emphasized.

The second part of the paper is dedicated to an application experiment in which the resonance curve of a tuning fork is finally recorded within several minutes of time and from affordable parts. Several principles and subtleties of signal acquisition and processing are encountered in this experiment; either for the generation of the excitation signals or for the processing of the recorded images. For instance, the trade-off between acquisition time and spectral resolution achieved; usually known as the uncertainty principle; is clearly observed in this experiment. This application work is also an opportunity to consider the Fourier theory in the spatial domain of two-

dimensional images instead of the time domain as often implemented in teaching works.

2. COMPUTER EXPLORATION OF THE DFT SIGNIFICANCE

2.1. Definitions

The following equations give the usual integrals of the continuous Fourier transform allowing to pass from the direct domain (variable x) to the reciprocal one (variable u) and vice-versa:

$$F(u) = \int_{-\infty}^{\infty} f(x)e^{-i2\pi ux} dx \quad (1)$$

$$f(x) = \int_{-\infty}^{\infty} F(u)e^{i2\pi ux} du \quad (2)$$

where functions $f(x)$ and $F(u)$ are Fourier transform of each other. In the case of discrete signals, the DFT is expressed as follows:

$$u_k = \sum_{n=1}^N x_n \exp \frac{-2\pi i}{N}(k-1)n, k = 1, \dots, N \quad (3)$$

$$x_n = \frac{1}{N} \sum_{k=0}^{N-1} u_k \exp \frac{-2\pi i}{N}(n-1), n = 1, \dots, N \quad (4)$$

where integers k and n stand for the indexes of the sample of the discrete signals. We chose a convention in which the N samples of the discrete signals are numbered with indexes from 1 to N as commonly used in computation softwares. Since the number N of samples is involved in the DFT definition, the indexes involved in these equations do not correspond directly to actual physical quantities. They are only linked to the actual physical quantities by two parameters; i.e. the number of samples N and the sampling frequency used for signal discretization. The following section emphasizes on the effect of the value of N on the Fourier spectrum finally obtained.

2.2. Observing the sampled frequency properties

In order to observe the effect of the number N of discrete samples on the Fourier spectrum obtained by DFT, we built a digital signal $s(i)$ simply made of a complex harmonic function whose frequency can be chosen arbitrarily as follows:

$$s(i) = \exp\left(j(\phi(i))\right) \quad \text{with:} \quad (5)$$

$$\phi(i) = 2\pi i/T + \phi_0 \quad (6)$$

where T is the period of the harmonic function and ϕ_0 is an arbitrary phase shift. The real and imaginary parts of this signal are plotted in 1. To observe the effect of N , we did not apply the DFT to the whole set of samples but only to a subset; i.e. on the interval defined by indexes I_{Left} through I_{Right} . The value of N is then varied by increasing the value of I_{Right} . Since $s(i)$ has a single frequency, we may expect the Fourier spectrum to be reduced to a single component. We can observe experimentally that this expectation is only verified for particular values of N whereas for the most common case, the Fourier spectrum is spread over a narrow band extending over several spatial components. To understand the origin of this behavior, let us consider Fig. 2 that corresponds to increasing values of N .

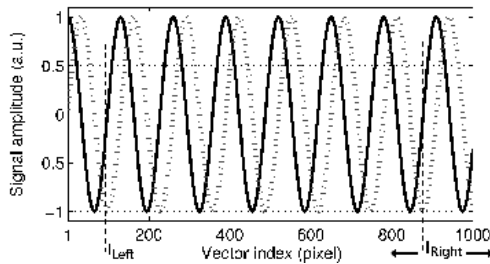


Figure 1: Harmonic signal used for simulation: real part; dotted imaginary part. A long period has been chosen for the sake of clarity. FFT is computed between I_{Left} and I_{Right} .

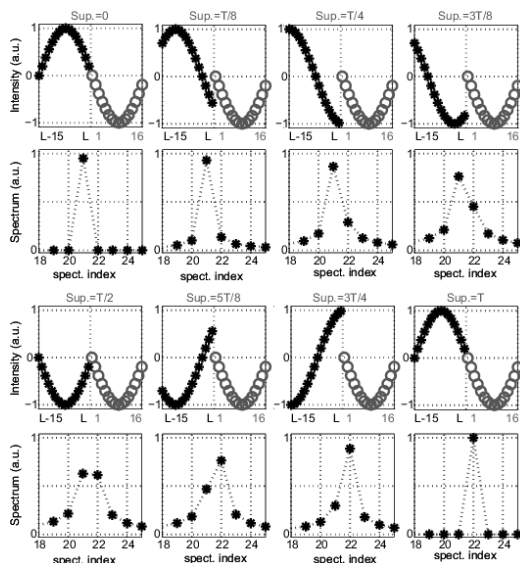


Figure 2: Relationship between vector length and Fourier power spectrum. Up: connection between end and beginning of vector data stars: last half period; circles: first half period); Bottom: Resulting Fourier power spectrum obtained. Sup. stands for the mismatch between vector length and closest multiple of periods.

It allows the visualization of the relationship existing between the length of the input signal and the shape of Fourier spectrum obtained. Eight different cases are represented by subset of two figures. For each subset, the upper sub-figure represents the extremities of the initial signal; i.e. its values as taken for the last sixteen samples (stars) and for the first sixteen samples (circles). Since I_{Left} is kept constant, the circles present the same curve in all sub-figures. At contrary, the stars present varying curves as a function of the value of I_{Right} . By observing the figures, we see that the Fourier spectrum is reduced to a single component when there is a perfect continuity between the end and the beginning of the interval considered. The following comments can be derived from these observations:

- When the Fourier spectrum is reduced to a single component, the input signal is equal to one elementary function of the DFT decomposition basis multiplied by a real coefficient. By varying the input signal frequency, the DFT decomposition function basis are identified by the values leading to a single component spectrum.
- The frequency of each DFT decomposition function corresponds to a particular value for which the N samples of the input signal form a whole number of periods. The law defining the sampled frequencies $f_k(k = 1, \dots, N)$ by:

$$f_k = \frac{k - 1}{N} \text{ per sample} \quad (7)$$

This law can also be expressed as: the k^{th} sampled frequency corresponds exactly to $(k - 1)$ periods for the N samples. This condition can be easily verified by setting $T = 1/f_k$ in Eq. 5 and 6. Whatever the value of N the spectrum is always made of a single component at index k .

- When this condition is satisfied, an infinite signal without phase jitter can be constructed artificially by juxtaposing identical sets of N samples. In such cases, the discrete form is qualitatively analogous to the definitions of equations 1 and 2 in the case of continuous functions.
- When this condition is not met, the input signal is decomposed onto a set of several sampled frequencies. The spectrum obtained is thus spread onto several components. We observe in the figure that the more pronounced the discontinuity, the wider the spectrum obtained.

The elementary computations proposed in this section constitute a convenient way to associate a visual representation with the mathematical definitions of the continuous and discrete Fourier transforms. The consequences of signal discretization are also emphasized.

2.3. DFT versus signal sampling theory

As well described in the signal sampling theory, the sampling of a continuous signal must comply with an important spectral bandwidth condition. This condition is known as Shannon theorem that requires the sampling frequency to be at least twice the highest frequency of the continuous signal. This condition can also be expressed by: *at least two samples per period* or by: *a maximum frequency of 0.5 per sample*. However, we observe in Eq. 8 that the sampled frequency becomes larger than 0.5 per sample for values of k larger than $N/2$. This means that the range of frequencies provided by a combination of signal sampling and DFT infringes the Shannon theorem. Despite this Shannon theorem infringement, the spectrum obtained by DFT is fully representative of the sampled signal. This contradiction results from the effect of signal sampling on the Fourier spectrum. Because of sampling, the initially band-limited spectrum of the continuous signal is convolved by a Dirac comb at the sampling frequency. The spectrum of the sampled signal is thus made of an infinite set of reproductions of the continuous signal spectrum. Each reproduction is representative of the continuous signal provided that there is no overlapping between the different spectrum reproductions. The latter condition is indeed the purpose of the Shannon theorem: if the signal bandwidth is narrower than half the sampling frequency there is no spectrum overlapping in the spectrum of the sampled signal. The way in which DFT accesses the signal. The way in which DFT accesses the signal spectrum is illustrated in Fig. 3(a). The continuous signal bandwidth is narrower than the interval $(f_s/2, f_s/2)$. After signal sampling, an infinite set of this spectrum is reproduced with a spacing of f_s . The frequency range provided by DFT extends on the interval $[0, f_s)$; i.e. on two consecutive reproductions of the spectrum of the continuous signal. However the initial spectrum of the continuous signal can be derived from the DFT one simply by applying a scale shift to the right part of the spectrum. The new sampled frequencies are then expressed by:

$$f_k = \frac{k-1}{N} - 1 \quad \text{per sample for } k = N/2, \dots, N \quad (8)$$

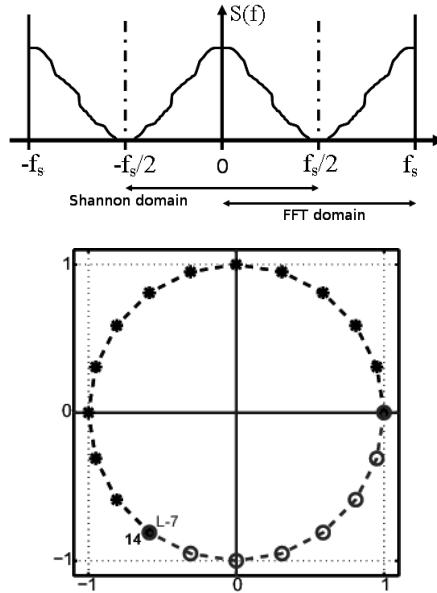


Figure 3: Up) Frequency domain of FFT computations with respect to the Shannon criterion domain; bottom) Phase shift per pixel for a given spectrum index (14). stars: $n < L/2$; circles: complementary phase with $n' < L/2$.

This translation of one half of the spectrum can be approached in a different way; i.e. visually on the trigonometric circle. The sampled frequencies correspond to 0 through $(N - 1)$ periods over the N signal samples and thus correspond to a total phase excursion of 0 through $(N - 1) \cdot 2$ rad. Reported to the transition from one signal sample to the next one, this equivalent phase excursion varies then from 0 through $\frac{N-1}{N} \cdot 2\pi$ rad. per sample. This is illustrated in Fig. 3(b) in the case of $N = 20$ for the sake of simplicity. Let us consider the case of $k = 14$. The phase excursion from one sample to the next one is marked by black stars and is equal to $13 \cdot \pi/10$ rad. We can observe that this phase excursion that is greater than π is equivalent to $-7 \cdot \pi/10$ rad. as marked by red circles. In the latter case, the phase excursion from one signal sample to the next one remains smaller

than as required by the Shannon theorem.

2.4. Significance of the Fourier phase

Although the Fourier phase is clearly defined by Eq. 1 and 3 its significance remains mysterious to many people, even among regular users of the Fourier transform. Figure 4 may help to understand visually the Fourier phase from elementary computations based on the input signal of Fig 1. To obtain Fig.4, we kept the number of samples N constant and simply shifted progressively the position of the analysis window by incrementing I_{Left} and I_{Right} simultaneously. We observe that while the first sample value describes one period, the

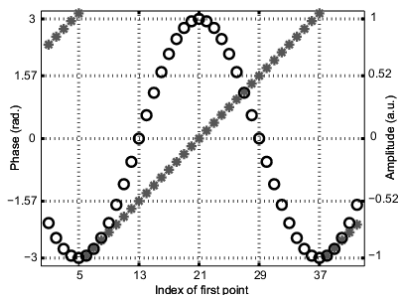


Figure 4: Relationship between spectral phase at Fourier power spectrum peak and the vector intensity at first data point. Red stars: spectral phase; black circles: first data point intensity.

Fourier phase of the peak component describes the $(\pi, \pi]$ interval. Furthermore we observe easily that the intensity of the first sample considered is directly given by the cosine of the Fourier phase. In addition to provide a visual representation of the Fourier phase, this figure demonstrates clearly how the Fourier phase can be used for displacement detection and measurement. Indeed, the motion of the analysis window with respect to the fixed input signal is equivalent to a translation of the input signal within the analysis window. The simultaneous observation on an oscilloscope of a cosine signal and of its delayed copy is a well known example of this property. In the

domain of imaging, we may consider a camera observing an object presenting a periodic contrast. Any lateral motion of the object induces a translation of the periodic contrast with respect to the image pixel frame that is equivalent to the conditions of Fig. 4. This displacement can thus be detected and measured by means of the Fourier phase with a conversion law of one period per 2π rad.

In the experimental part of this paper, we apply this property of the Fourier phase to the characterization of the resonance curve of a tuning fork. We may notice that we proposed a quite similar experiment in a previous work (Sandoz, Friedt, Carry, Trolard, y R., 2009) but the present work differs in several ways.

Here we use a periodic pattern stuck on the prong end of the tuning fork. A single spectral component has thus to be considered and computations can be performed at video-rate. We do not implement a quite complicated iterative algorithm to reconstruct the prong end displacement since it is directly given by the Fourier phase variation observed. However, the Fourier phase observed here is subject to a 2π uncertainty and thus allows only the measurement of vibration amplitudes smaller than half a period of the pattern stuck on the prong end. As demonstrated below, the tuning fork resonance can be reconstructed despite this limitation with the interest that it can be obtain within a couple of minutes instead of hours in the method reported previously.

3. APPLICATION TO VIDEO-RATE TUNING-FORK VIBRATION AMPLITUDE MEASUREMENT

3.1. Tuning-fork excitation and observation

The relationship explained in previous sections between a displacement in the signal domain and a phase change in the spectral domain has been applied to the development of an affordable instrumentation setup. The latter is dedicated to the characterization of the vibration amplitude of a tuning-fork. The experimental setup is shown in Fig.5. It combines excitation and imaging of the tuning-fork

and is fully controlled by a laptop computer. Tuning-fork excitation is obtained by magnetic coupling between a speaker located close to the end of one prong and the ferromagnetic material of the tuning-fork (Sandoz y cols., 2009). The speaker driving signal is synthesized numerically and sent to one channel of the stereo sound card of the computer. The second sound channel is used in the same way for

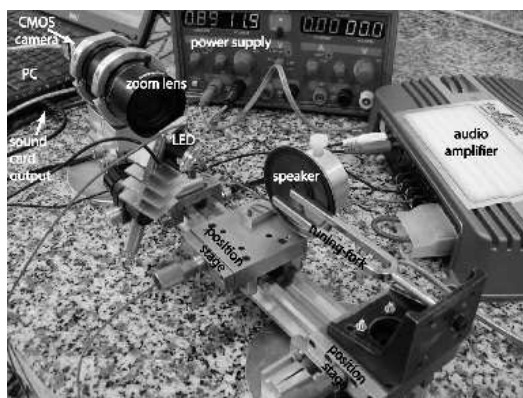


Figura 5: Experimental setup used for tuning-fork vibration amplitude measurement.

monitoring a pulsed LED (LXHL-MWEA White Luxeon®Star/C) illuminating the prong-end surface. A two-channel audio amplifier (Sony®XM-SD12X250W) amplifies the sound card outputs to the levels required for driving the LED and the speaker. Since the tuning-fork natural-frequency is much larger than the standard video-rate, a stroboscopic illumination is necessary to perform a frequency change. In this aim a 1.25 Hz frequency shift is systematically applied between the excitation signals of the speaker and of the LED. The motion of the tuning-fork is thus observed with an apparent frequency of 1.25 Hz that is compatible with the bandwidth of a standard camera. The vision system used is made of a CMOS camera (μ Eye UI-1540-M) connected to the USB port of the personal computer and a C-mount zoom lens (*Computar* MLH-10x). In practice the continuous excitation of the tuning fork is obtained by the infinite repetition of

a time-limited signal of duration T sent digitally to the sound card memory. To be equivalent to a steady-state harmonic signal, this infinite repetition of a time-limited sequence must ensure the perfect phase continuity between the consecutive sequences. This condition requires that the duration T is equal to an entire number of period of the synthesized frequency as illustrated in Fig.2. The relationship between the resolutions achieved in the direct and reciprocal domains is then easily derived from this requirement:

$$T \cdot f = k \quad \text{and} \quad T \cdot (f + \delta f) = k + 1 \quad (9)$$

By subtracting these equations, we derive the frequency resolution δf allowed by a duration T as well as the minimum duration T for exploring the frequency domain with a given resolution δf :

$$\delta f = 1/T \quad \text{or} \quad T = 1/\delta f \quad (10)$$

From a discretization point of view, the duration T has to be a multiple of the sampling period of the discrete signal built digitally in order to avoid any phase jitter between the consecutive sequences. In practice the sampling frequency can be adjusted as a function of the desired frequency in order to fulfil this continuity requirement.

A periodic pattern of lines is stuck on the prong-end surface in the aim to provide a carrier frequency on which phase computations can be performed similarly to simulations carried out previously. Fig.6 presents an image of the periodic pattern of lines as recorded experimentally. In practice, we used a simple piece of paper on which a half tone of gray has been printed. Shades of gray are indeed obtained by periodic distributions of black spots or lines. The intensity of gray is controlled through the distribution duty cycle while its period remains constant; at a value sufficiently small to be cut-off by the naked-eye bandwidth. In the figure, the vertical lines correspond to a 25 % gray level while the oblique border line corresponds to a gray level of 50 %. The lines between 100-200 define a working interval of 100 lines used as input data for image processing. In fact all lines in this set carry the same spectral information but each one with an independent pattern of noise due to printing imperfections and electronic noise. By summing these 100 lines along columns, we

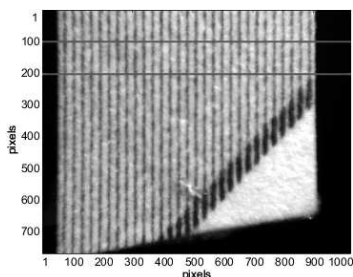


Figura 6: Recorded image of the line pattern stuck on the prong end of the tuning-fork. The lines define the region of interest actually recorded.

obtain a noise-averaged signal as represented in Fig7. in which the carrier frequency appears clearly with a high signal-to-noise ratio. Any vibration of the tuning-fork; i.e. any displacement of the prong-end surface; can therefore be detected by analyzing the position of this carrier-frequency signal with respect to the pixel frame of the camera as described in the next section.

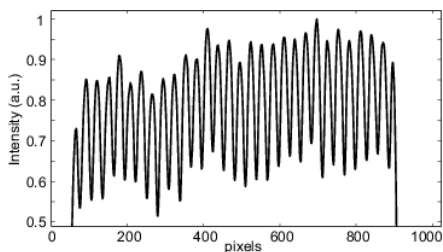


Figura 7: Sum of one hundred lines of linearly-patterned image of the prong-end surface.

3.2. Fourier phase analysis and vibration amplitude reconstruction.

A vibration of the tuning-fork induces a lateral shift of the periodic pattern printed on the prong-end surface in front of the vision system. This vibration induces thus in the recorded image a displacement of the carrier-frequency signal with respect to the pixel frame of the camera. The aim of the signal processing is therefore to follow the lateral position of this carrier-frequency signal along the image column-index frame. As explained before, this information is provided by the Fourier phase of the DFT taken at the particular frequency of interest. We work in this way but in practice, we made two specific adjustments:

- In order to save time and to achieve real-time processing, we compute a single spectral component instead of performing a complete DFT.
- To avoid disturbances due to the limited extension of the line pattern, we choose to perform a windowed Fourier transform as shown by the analysis function of Fig.8. The latter has a gaussian envelope and its frequency is equal to that of the line pattern in the recorded images.

The expected Fourier phase is thus obtained through the following sum:

$$S = \sum s_i \cdot a_i \quad \text{and} \quad \phi = \text{angle}(S) \quad (11)$$

where i is the column index, s_i is the sum of one hundred lines of the recorded image, a_i is the analysis function represented in Fig.8 and ϕ is the Fourier phase. The computation of this equation is not time-consuming and the tuning-fork vibration amplitude can be displayed at video-rate. Fig.9 presents the evolution of the Fourier phase versus time after switching on the tuning-fork excitation at the resonance frequency. The signal oscillations are due to the 1.25 Hz phase difference between the excitation and stroboscope frequencies while its envelope corresponds to the vibration amplitude. We observe the progressive increase of the vibration amplitude up to the

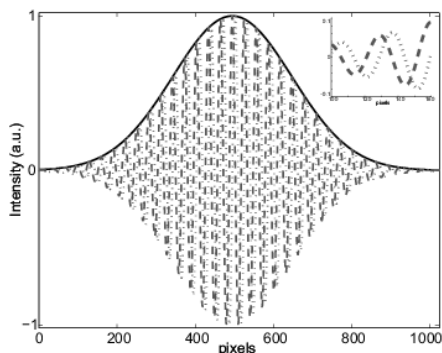


Figure 8: Fourier phase analysis function; black: window envelope; dashed: real part; dotted : imaginary part. Phase quadrature can be seen in the zoom presented in the inset.

steady-state regime. This measurement is obtained in radians with a conversion rule of 2π per pattern period. The actual calibration in micrometer assumes the calibration of the vision system through the measurement of the pattern period or by means of a reference object. In our case, the displacement was evaluated to be $27 \mu\text{m}$ per radian for a pattern frequency of 5.9 mm^{-1} .

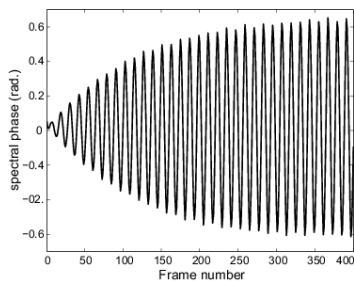


Figure 9: Spectral phase versus time for a tuning-fork excitation at resonance frequency.

The phase variation observed in Fig.9 is centered on a mean phase value π_0 that depends on the pattern position in absence of vibra-

tion. π_0 can take any value in the interval $(-\pi, \pi]$. If ϕ_0 is close to $\pm\pi$, 2π phase discontinuities may appear. The latter can be removed afterwards by performing a phase unwrapping. They can also be prevented by inserting a phase offset in the analysis function in order to set $\phi_0 = 0$. If the vibration amplitude becomes larger than π , this precaution does not work anymore and phase unwrapping has to be performed.

By scanning step by step the excitation frequency we recorded the tuning-fork resonance curve as represented in Fig.10. We choose a frequency step of 0.05 Hz and we respected a temporization of 20 s to wait for the steady-state to be established. Another 20 s temporization is also used for vibration damping before switching to the next frequency value. In this way the resonance curve of Fig.10 was recorded automatically in about 25 mn . This time lapse can still be reduced by restricting the explored spectrum to the central part of the resonance curve. Such a recording can thus be carried out by the end of a laboratory course.

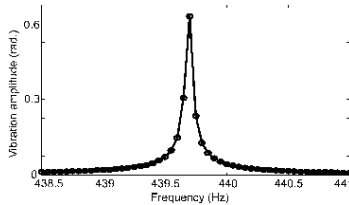


Figura 10: Resonance curve of the tuning-fork as obtained from spectral phase variation amplitude measured at video-rate.

4. CONCLUSION

This paper proposes a “hands on” approach to the Fourier transform with an emphasize on the different effects of signal discretization. The elementary simulations of the first part help to get a visual representation of how the DFT works and to understand the importance of the number of signal samples considered as well as of the

effects of frequency sampling on the spectra obtained. The significance of the Fourier phase may also be clarified. The second part of the paper proposes an application experiment leading to the recording of the resonance curve of a tuning fork within a couple of minutes. The setting up of this experiment assumes that basic principles such as stroboscopy for instance are understood. Once the experiment and the software are ready, they can be used for further exploration of the tuning fork behavior as proposed elsewhere (Sandoz y cols., 2009). The completion of this work would be an interesting subject since it covers many aspects of a detection chain in addition to digital aspects of signal generation and numerical simulations. The affordable cost of the required hardware could still be reduced by working with a webcam and an homemade imaging system.

Referencias

- Chen, X., Huang, J., y Loh, E. (1988). Two-dimensional fast fourier transform and pattern processing with ibm pc. *Am. J. Phys*, 56, 747.
- D'Astous, Y., y Blanchard, M. (1982). Properly used "aliasing" can give better resolution from fewer points in fourier transform spectroscopy. *Am. J. Phys*, 50, 464.
- Higgins, R. J. (1976). Fast fourier transform: An introduction with some minicomputer experiments. , 44, 766.
- Kocher, C. A. (1988). Experiments with fourier transforms at radio frequencies. *Am. J. Phys*, 56, 524.
- Lambert, R. K., y O'Driscoll, R. C. (1985). Fourier series experiment for the undergraduate physics laboratory. *Am. J. Phys*, 53, 874.
- Maas, P. (1978). Discussion of the use of fast fourier transform for spectral analysis. *Am. J. Phys*, 46, 857.
- Matthys, D. R., y Pedrotti, F. L. (1982). Fourier transforms and the use of a microcomputer in the advanced undergraduate laboratory. *Am. J. Phys*, 50, 990.
- Oppenheim, A., y Schafer, R. (1975). *Digital signal processing*. Prentice Hall.

- Peters, R. D. (1992). Fourier transform construction by vector graphics. *Am. J. Phys*, 58, 439.
- Sandoz, P., Friedt, J., Carry, E., Trolard, B., y R., J. G. (2009). Frequency domain characterization of the vibrations of a tuning fork by vision and digital image processing. *Am. J. Phys*, 71, 20.
- Whaite, G., y Wolfe, J. (1990). Harmonic or fourier synthesis in the teaching laboratory. *Am. J. Phys*, 58, 481.

